Software Tools for Uncertainty Evaluation in VNA Measurements: A Comparative Study*

G. Avolio[1], D. F. Williams[2], S. Streett[2], M. Frey[2], D. Schreurs[1], A. Ferrero[3], M. Dieudonné[3]
[1]KU Leuven, Belgium, [2]NIST, Boulder (CO), USA, [3]Keysight Technologies Inc (CA), USA

***Abstract* — We compared three software tools designed for scattering-parameter measurement uncertainty evaluation. These tools propagate uncertainty to calibrated S-parameters by means of a sensitivity analysis. We also validated the sensitivity analysis with Monte-Carlo simulations performed with one of the software tools and the Keysight ADS circuit simulator.**

***Index Terms* — Microwave measurements, Monte-Carlo simulations, sensitivity analysis, S-parameters, uncertainty.**

I. Introduction

There have been a number of recent efforts in both academia and industry to develop software tools to quantify uncertainty in scattering- (S-) parameter measurements and other quantities at microwave frequencies [1]-[6]. For example, a comparison of existing software tools was conducted by Teppati *et al.* in [7].

Along the lines of [7], we compare three software packages. The first two packages represent the Microwave Uncertainty Framework (MUF) [2]-[3], developed by the National Institute of Standards and Technology (NIST) in the United States, and VNA Tools II [4]-[5], developed by the Swiss Metrological Institute (METAS). The third package is an implementation† of the work in [6]. In what follows we will refer to the third package as 'SW3'. All of these software tools carry out uncertainty propagation by means of a sensitivity analysis, each using a slightly different approach. The NIST tool also simultaneously performs a Monte-Carlo analysis that maintains correlations throughout the process of determining and propagating uncertainties.

To evaluate the three software tools, we calibrated VNA measurements and propagated uncertainties in the calibration standards to the corrected S-parameters of an attenuator. Physical models of the calibration standards have been developed and verified by NIST [8]. These models include tolerances in their electrical characteristics and mechanical dimensions, thus allowing traceable uncertainty analysis.

II. Software-Tool Overview

While the detailed description of how the three software tools perform uncertainty analysis is beyond the scope of this paper, a general overview helps to better understand our experimental results. Given a model for a measurement:

$$\underline{Y} = \boldsymbol{f}(\underline{X}), \tag{1}$$

with X being a vector of input quantities with uncertainty, an estimate of the covariance matrix of the vector of output quantities Y can be computed by

$$\sum_Y = \underline{J} \sum_X \underline{J}^T , \tag{2}$$

where $\sum_X$ is the estimated covariance matrix of the input quantities and J is the Jacobian matrix of f [9]. Equation (2) is the result of a first-order approximation of (1). In the context of VNA measurements, $\sum_X$ typically accounts for uncertainties in the calibration standards definition, repeatability, and instrument noise.

The NIST MUF approximates J with a finite-difference approach [2]. In VNA Tools II, J is calculated by a method based on automatic differentiation [1]. SW3 derives J analytically [6].

A. Calibration standards

To run the NIST MUF, the user inputs models of the calibration standards along with tolerances in the mechanical dimensions and electrical properties of those models. We built the covariance matrix $\sum_Y$ of each calibration standard, in a format compatible with METAS VNA Tools II (*.sdatcv* format) and SW3 (*.dsd* format), starting from models available in the NIST MUF. We generated $\sum_Y$ by using (2), with $\sum_X$ being a diagonal matrix with uncertainties associated with the mechanical tolerances and electrical properties, and f the function describing the model of each of the calibration standards. If correlations across frequencies are also needed [10], [11], we could add them when generating $\sum_Y$. We did not populate $\sum_Y$ with those correlations since in this work we looked at S-parameters at each frequency separately. However, with the current version of these software packages, only the NIST MUF and METAS VNA Tools II can account for correlations across frequencies.

B. Noise and repeatability

Both noise and cable and connector repeatability can be accounted for in the three software tools. The NIST MUF accounts for noise by averaging repeated measurements. In METAS VNA tools II the user can define the VNA noise floor and the trace noise [7]. In SW3, the covariance matrix for noise

* Work partially supported by US government, not protected by US copyright.
† The US National Institute of Standards and Technology does not endorse commercial products. Other products may work as well or better.

978-1-5386-2747-1/17/$31.00 ©2017 IEEE

is estimated by repeated measurements of a matched and reflective DUT [6].

As in our analysis, we were interested in comparing three uncertainty evaluation methods. We included for simplicity only systematic uncertainties in the calibration standards definition and neglected uncertainties due to noise and repeatability.

In Table I we summarize the main features of the three software packages.

TABLE I: MAIN FEATURES OF THE THREE SOFTWARE PACKAGES

	NIST MUF	METAS VNA Tools II	SW3
Sensitivity Analysis	✓	✓	✓
Monte-Carlo Analysis	✓		
Speed	+	++	+++*
Frequency Correlations	✓	✓	

*Notably for multiport calibrations

III. EXPERIMENTAL RESULTS

A. Nominal calibration

We used Keysight PNA-X software to perform coaxial measurements from 200 MHz to 44 GHz with 30 Hz resolution bandwidth. We fixed cables and minimized cable movement between each measurement as best as we could. We used a 2.4 mm commercial calibration kit with corresponding NIST models [8]. In total we included 68 uncertainty sources. We calibrated the S-parameters of a 20 dB attenuator with an unknown-thru algorithm (S-O-L-R) [12]. We used physical models for the open and short standards. For the load we used a measurement based model, traceable to a coaxial multiline thru-reflect-line (TRL) calibration [8].

In Fig. 1, we show the calibrated magnitude and phase of the S_{11} and S_{21} parameters of our DUT. In Fig. 2, we also report the difference between these values. While we were able to use the same raw input data to calibrate the data with the NIST MUF and METAS VNA Tools II, we did not have access to raw data used by SW3 during the calibration procedure. In Fig. 2 we observe that the difference between the magnitude and phase of S_{11} and S_{21} as calibrated by the NIST MUF and METAS VNA Tools II is negligible. Note that the difference in the raw input data affects not only the calibrated S-parameters (1), but may also change the results of the sensitivity analysis (2). The matrix J (2) contains the partial derivatives of Y versus X calculated at the nominal value of all the quantities in X, and, therefore, J is a function also of the raw input data.

B. Sensitivity analysis

We show the results of the sensitivity analyses computed by the three software tools in Fig. 3 and the difference between the calculated uncertainties in Fig. 4. Any difference observed in the estimated uncertainty should be mainly ascribed to the method utilized to compute the J matrix. In our study, this was the case for the uncertainty computed by the NIST MUF and the METAS VNA Tools II, as we inputted exactly the same raw data into both tools. (Recall that the NIST MUF computes partial derivatives by means of a finite-difference approximation and METAS VNA Tools II employs an automatic differentiation method [1]-[13].)

On the other hand, the slight disagreement between the uncertainty estimated by NIST MUF or METAS VNA Tools II and SW3 may be due to the difference between the raw input data used for calibration, especially at higher frequencies. Nevertheless, we see that at lower frequencies, where there is less discrepancy between raw input data (see Fig. 2), the METAS VNA Tools II and SW3 sensitivity analyses agree better with each other than they do with the NIST MUF. As expected, depending on the shape of the function f in (1), the finite-difference approximation adopted by NIST MUF to calculate J (2) might be somewhat less accurate than the analytic approach used in SW3 [6] or the automatic differentiation approach used in the METAS VNA Tools II [13].

IV. MONTE-CARLO SIMULATIONS

A sensitivity analysis relies on a first-order approximation of (1). If f is nonlinear, the covariance matrix estimated by (2) will incompletely describe the uncertainties and their probability distributions. The NIST MUF uses Monte-Carlo simulations to assess the more complex uncertainties and probability distribution functions that result when f is nonlinear.

Here we use the built-in Monte-Carlo simulations in the NIST MUF to examine the results of the sensitivity analyses that are exclusively relied on by the other two software packages. This is not only a standard way of verifying the validity of sensitivity analyses [14], but lends insight into the differences between the approaches for estimating uncertainties.

A. Comparison of Monte-Carlo and Sensitivity Analyses

We performed a Monte-Carlo analysis with the NIST MUF, which uses a built-in random-number generator and specially generated seeds to maintain correlations. By using Monte-Carlo simulations, the average and standard deviation of Y can be estimated by evaluating (1) directly as a function of randomly generated realizations of vector X. When f is strongly nonlinear, the distribution of Y is no longer normal.

In Fig. 5 we compare the uncertainty estimated by sensitivity analysis to that from 1000 Monte-Carlo simulations. The two analyses agree reasonably well over many frequency ranges, but clearly do not agree at all frequency points. In particular, there is a clear discrepancy in the uncertainty of the magnitude of calibrated S_{21}. Moreover, the histogram shown in the inset of Fig. 5c, clearly indicates that the distribution of the magnitude of S_{21} at 44 GHz is not normal, as expected by sensitivity analysis.

B. Verification of the Monte-Carlo Analyses

To verify the correctness of our Monte-Carlo analysis, we ran the same calibration and performed Monte-Carlo simulations both in the NIST MUF and in a commercial circuit simulator (Keysight ADS). For the sake of simplicity, we considered one source of uncertainty, instead of 68 uncertainty sources included in our original calibration. We then performed a more in-depth investigation and found that, by considering only the uncertainty in the electrical conductivity of the coaxial line used to model the open standard, we could reproduce a situation similar to that in Fig. 5 based on the same raw data from the original calibration. We set the electrical conductivity to the same nominal value and distribution that we used for the original calibration, namely 5 MS/m, and a uniform distribution with support between 1 MS/m and 9 MS/m. We ran 1000 Monte-Carlo simulations with both the NIST MUF and Keysight ADS, and compared the estimated uncertainties. We repeated Monte-Carlo simulations with Keysight ADS by increasing the number of iterations to 5000 and did not observe any significant change in the results.

As in the original calibration, we observed disagreement between the uncertainty estimated by Monte-Carlo simulations and sensitivity analysis, particularly for the magnitude of the calibrated S_{21} (Fig. 6). For this quantity, we show the histogram obtained by Monte-Carlo simulations at 44 GHz in Fig. 7. First, we observe that the histograms obtained with the NIST MUF and Keysight ADS are very similar (see also Appendix). Most significantly, the shape of those histograms clearly shows that the underlying probability distribution is not normal.

C. Origin of the discrepancy

We also investigated the origin of the disagreement in Fig. 6 and the histograms asymmetry in Fig. 7a. Since the electrical conductivity was the only input variable with uncertainty in the simplified calibration, we looked at the dependence on this variable of the magnitude of the calibrated S_{21} at 44 GHz.

The dependence of S_{21} is nonlinear, as shown in Fig. 7b. When running Monte-Carlo simulations, the electrical conductivity varies over a large range, based on the support of its probability distribution function. Looking at Fig. 7b, in the low-loss region, the magnitude values of S_{21} saturate, as opposed to the high-loss region, where dependence on the electrical conductivity is greater, creating the asymmetric shape of the histograms in Fig. 7a. Thus, we see that a sensitivity analysis, which relies on a linearization around the nominal value (see Fig. 7b), poorly captures these large variations and inaccurately estimates uncertainty.

To further corroborate our analysis, we show in Fig. 7a an approximate probability density function (*pdf*), derived analytically (as explained in the Appendix).

V. Conclusions

We compared three software tools which compute uncertainty in S-parameter measurements at microwave frequencies. These tools propagate uncertainty based on a sensitivity analysis and, despite the fact that they utilize different methods to perform their sensitivity analyses, the estimated uncertainties agree very well. However, sensitivity analysis relies on a first-order approximation, which is not always valid. When this occurs, Monte-Carlo simulations should be used in lieu of sensitivity analysis, since the sensitivity analysis results will be inaccurate.

Acknowledgement

This work was partially supported by Keysight Technologies Belgium. G. Avolio is supported by FWO Vlaanderen (Belgium). Authors would like to thank J. A. Jargon, J. Wang, and A. Koepke for useful discussions.

Appendix

In Fig. 7a we show an approximate *pdf* of the magnitude of S_{21}. The magnitude of S_{21} is linked to the electrical conductivity by a quite complicated function. However, in order to qualitatively validate our Monte-Carlo results, we approximated that complicated expression with a simpler function allowing us to derive analytically the *pdf* associated with this function. The comparison between the original and fitted function is shown in Fig. 8a. In Fig. 8a, the fitted function is

$$Y = A + B * \operatorname{atan}[C * (X + D)] , \tag{A.1}$$

where, in our case, Y is the magnitude of S_{21} and X the electrical conductivity. Given the *pdf* of X, if Y is a monotonic function of X, then the *pdf* of Y is equal to

$$pdf(Y) = pdf(X)\frac{dX}{dY} , \tag{A.2}$$

where *pdf(X)* is the *pdf* of the electrical conductivity which is constant for a uniform distribution. By applying (A.2) to (A.1), we can straightforwardly derive the *pdf(Y)* as:

$$pdf(Y) = \frac{pdf(X)}{C * B}\left(1 + tan^2\left(\frac{Y - A}{B}\right)\right), \tag{A.3}$$

which is plotted in Fig. 7a.

In Fig. 8b we show a quantile-quantile plot (q-q plot) to graphically assess the similarity between the probability distributions underlying the two histograms in Fig. 7a. The samples from Monte-Carlo simulations performed with the NIST MUF and Keysight ADS align quite well with the unitary-slope ideal line which the samples would lie on if the two histograms were exactly the same.

References

[1] B. D. Hall, "Calculating measurement uncertainty using automatic differentiation," *Meas. Sci. Technol.*, vol. 13, no. 4, pp. 421–427, 2002.

[2] A. Lewandowski, D. Williams, P. Hale, C. M. Wang, and A. Dienstfrey, "Covariance-matrix-based vector-network-analyzer uncertainty analysis for time-and frequency-domain measurements," *IEEE Trans. Microw. Theory Techn.*, vol. 58, no. 7, pp. 1877-1866, Jul. 2010.
[3] [Online]. Available: https://www.nist.gov/services-resources/software/wafer-calibration-software.
[4] M. Wollensack, J. Hoffmann, J. Ruefenacht, and M. Zeier, "VNA tools II: S-parameter uncertainty calculation," in *Proc. 79th ARFTG Conf.*, Montreal, QC, Canada, Jun. 2012, pp. 1–5.
[5] M. Wollensack and J. Hoffmann. (2012, Apr.). METAS VNA Tools II-Math Reference [Online]. Available: http://www.metas.ch/vnatools.
[6] M. Garelli and A. Ferrero, "A unified theory for S-parameter uncertainty evaluation," *IEEE Trans. Microw. Theory Techn.*, vol. 60, no. 12, pp. 3844-3855, Dec. 2012.
[7] V. Teppati and A. Ferrero, "A comparison of uncertainty evaluation methods for on-wafer S-parameter measurements," *IEEE Trans. Instrum. Meas.*, vol. 63, no. 4, pp. 935-942, Apr. 2014.
[8] J. A. Jargon, C. Cho, D. F. Williams, and P. D. Hale, "Physical models for 2.4 mm and 3.5 mm coaxial VNA calibration kits developed within the NIST microwave uncertainty framework," *85th Microwave Measurement Conference (ARFTG)*, pp. 1-7, 2015.
[9] N. M. Ridler and M. J. Salter, "Propagating S-parameter uncertainties to other measurement quantities," *58th Microwave Measurement Conference (ARFTG)*, vol. 40, pp. 1-9, 2001.
[10] D. F. Williams, "Covariance-based uncertainty analysis of the NIST electroptic sampling system," *IEEE Trans. Microw. Theory Techn.*, vol. 54, no. 1, pp. 481-491, Jan. 2006.
[11] G. Avolio, A. Raffo, J. A. Jargon, P. D. Hale, D. M. M. -P. Schreurs, and D. F. Williams, "Evaluation of Uncertainty in Temporal Waveforms of Microwave Transistors," *IEEE Trans. Microw. Theory Techn.*, vol. 63, no. 7, pp. 2353-2363, Jan. 2015.
[12] A. Ferrero and U. Pisani, "Two-port network analyzer calibration using an unknown 'thru'," *IEEE Microw. Guided Wave Lett.*, vol. 2, no. 12, pp. 505–507, Dec. 1992.
[13] R. Boudjemaa, M. G. Cox, A. B. Forbes, and P. M. Harris, "Automatic differentiation and its application in metrology," *Advanced Mathematical and Computational Tools in Metrology VI*, pp. 170 – 179, Italy, 2003.
[14] B. D. Hall, "Evaluating methods of calculating measurement uncertainty," *Metrologia*, vol. 45, n. 2, pp. 1-5, 2008.

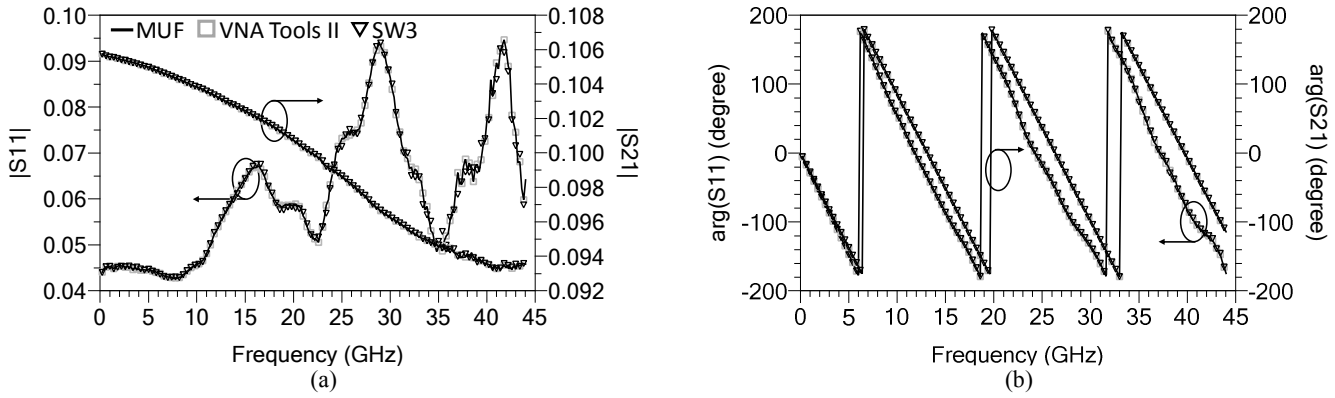

Fig. 1: S-O-L-R calibrated magnitude (a) and phase (b) of S_{11} (left Y-axis) and S_{21} (right Y-axis) of a 20 dB attenuator: NIST MUF (continuous line), METAS VNA Tools II (squares), and SW3 (triangles).

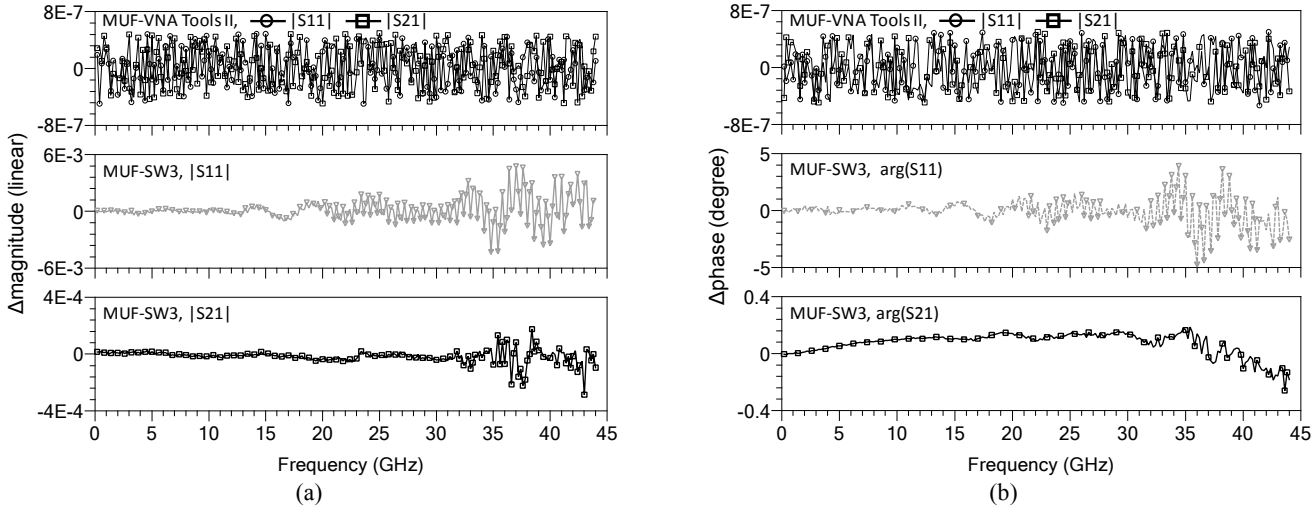

Fig. 2: Difference between magnitude (a) and phase (b) of S_{11} and S_{21} of a 20 dB attenuator calibrated with the three software tools. In both (a) and (b) the top plot shows the difference between the NIST MUF and METAS VNA Tools II, for which we inputted exactly the same raw data. The middle and bottom plots show the difference between the magnitude (a) and phase (b) of S_{11} and S_{21} computed by the NIST MUF and SW3.

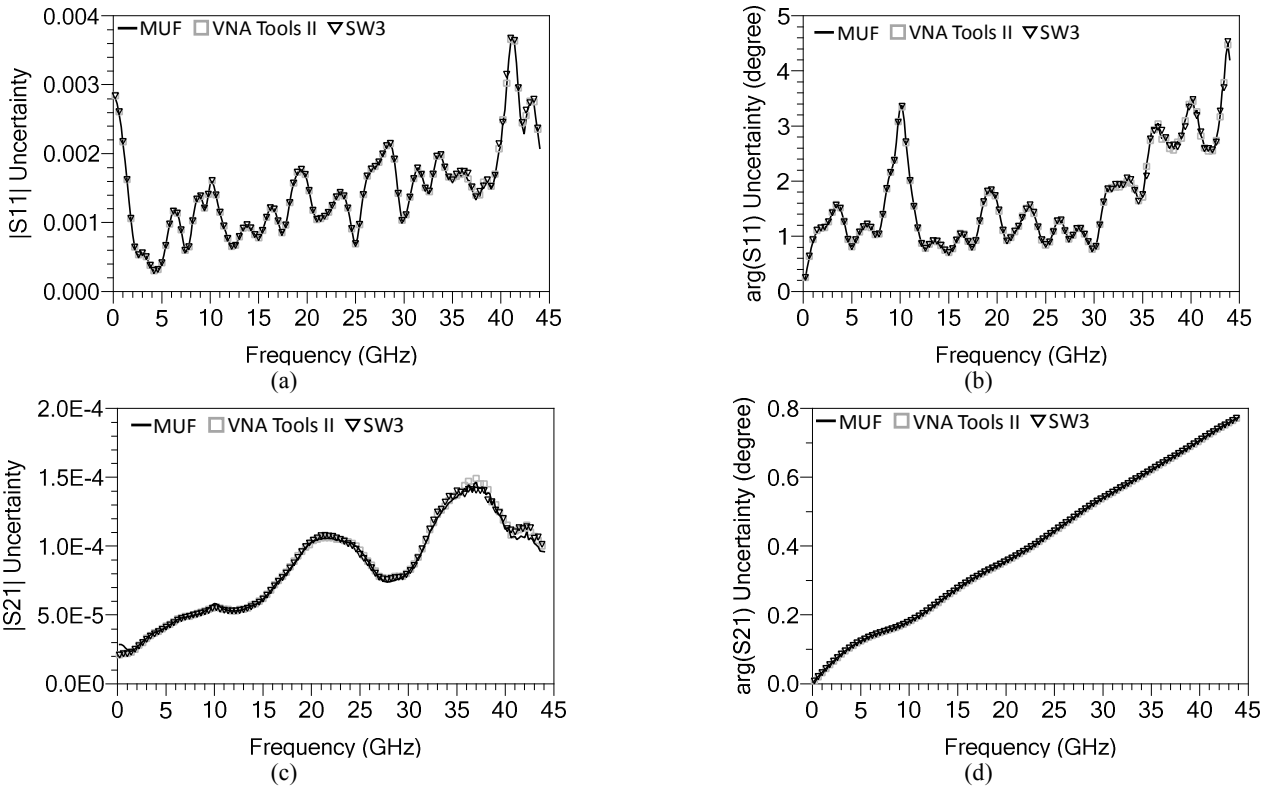

Fig. 3: Standard uncertainty estimated by the three software packages' sensitivity analyses. Magnitude and phase of S_{11} (a)-(b) and of S_{21} (c)-(d).

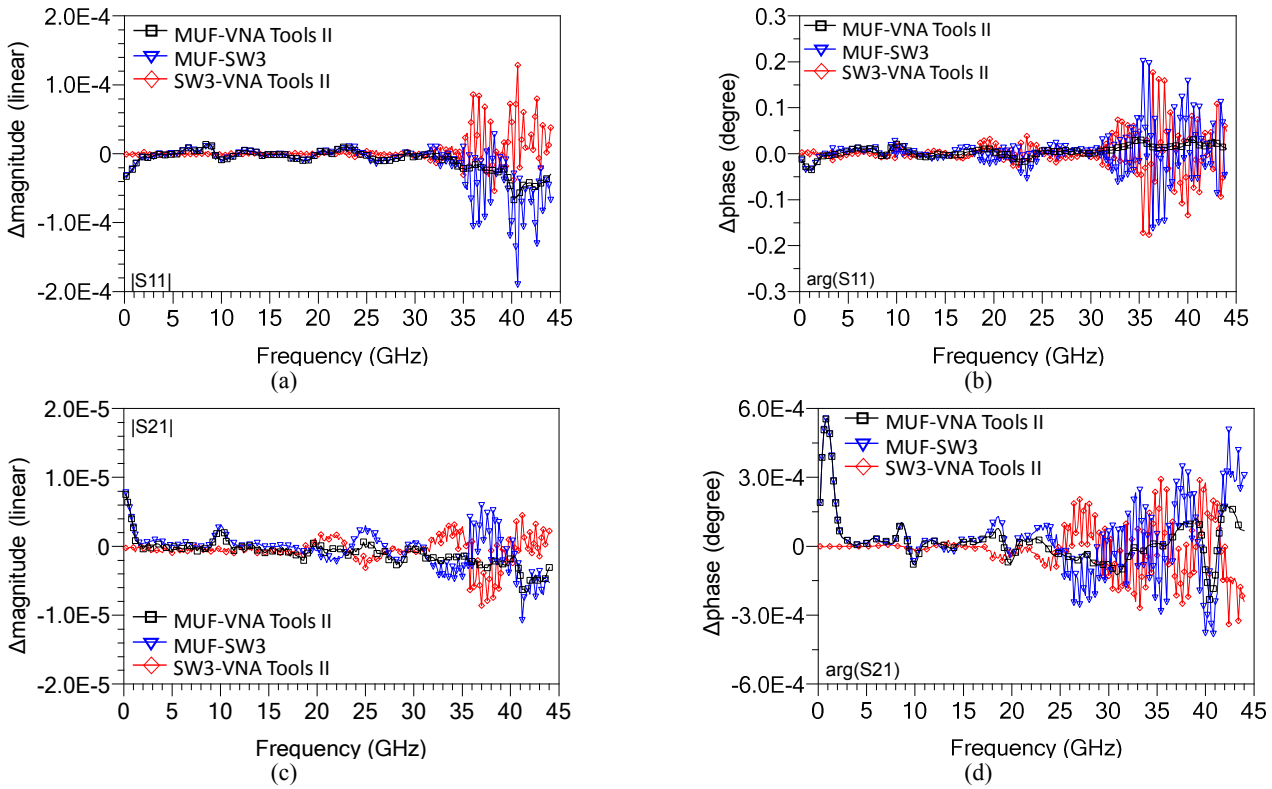

Fig. 4: Difference between the standard uncertainty in magnitude and phase of S_{11} (a)-(b) and S_{21} (c)-(d).

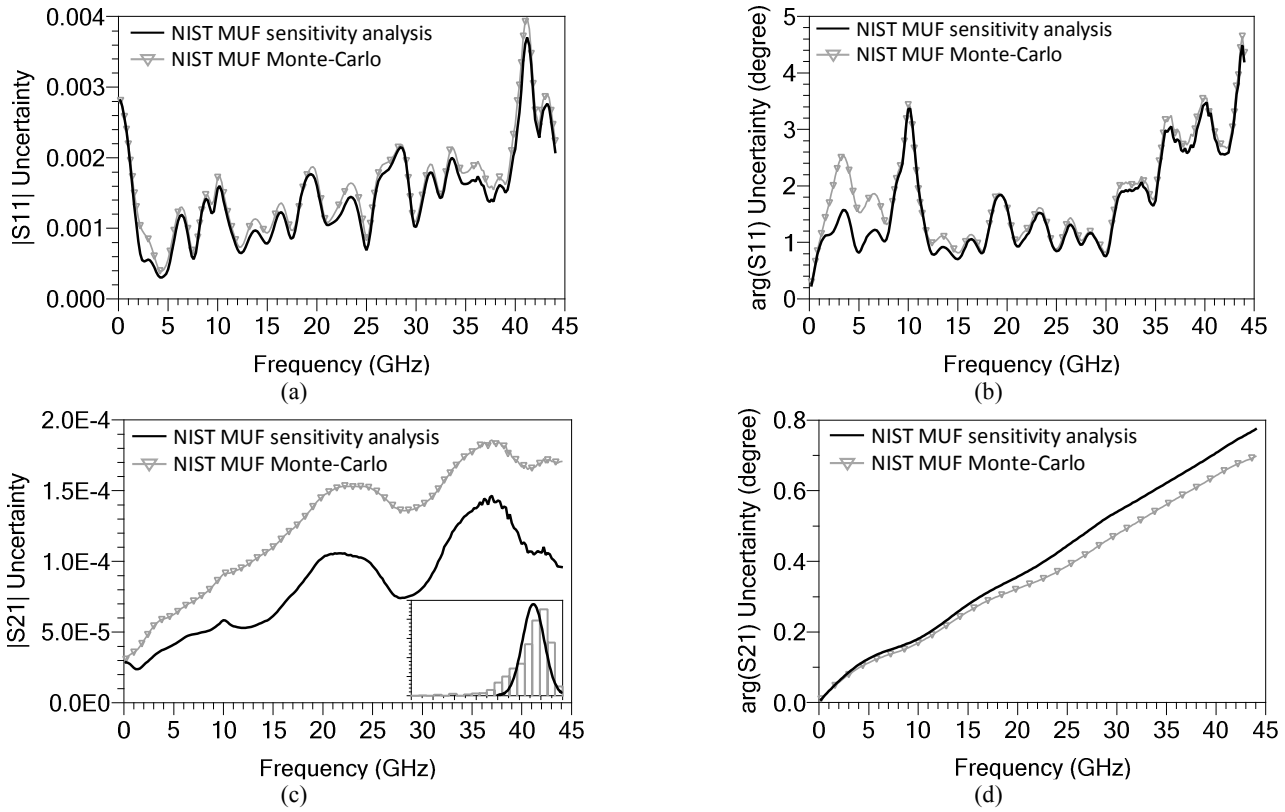

Fig. 5: Uncertainty in the calibrated magnitude and phase of S_{11} (a)-(b) and S_{21} (c)-(d) estimated by sensitivity (continuous line) and Monte-Carlo (symbols) analyses performed by the NIST MUF. The inset to Fig. 5c shows the distribution of the magnitude of S_{21} at 44 GHz resulting from Monte-Carlo (grey) and sensitivity (black) analyses.

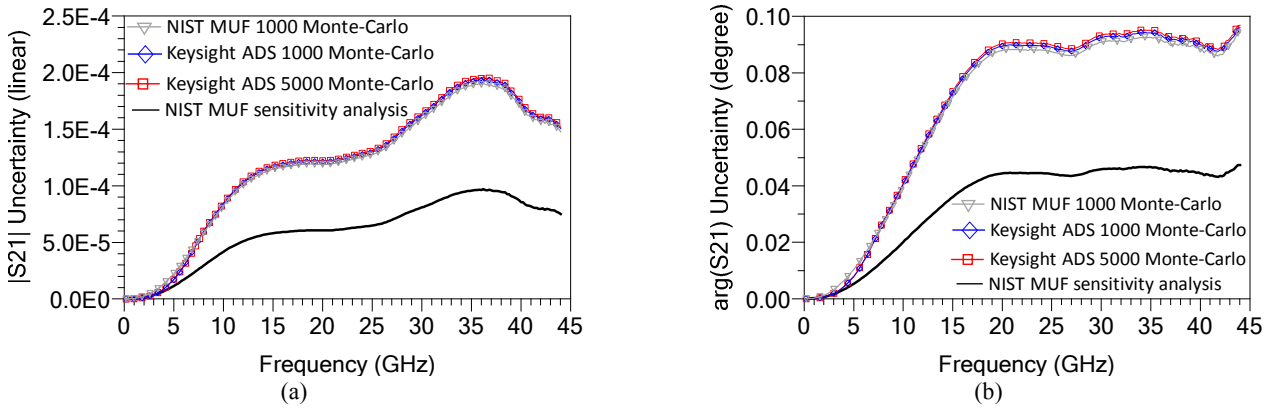

Fig. 6: Uncertainty estimated by Monte-Carlo simulations executed with the NIST MUF (triangles) and a commercial circuit simulator (diamonds and squares) and uncertainty estimated by the NIST MUF sensitivity analysis (continuous line). Raw data were S-O-L-R calibrated both in the NIST MUF and the commercial software and only one uncertainty contribution was propagated to the calibrated S-parameters.

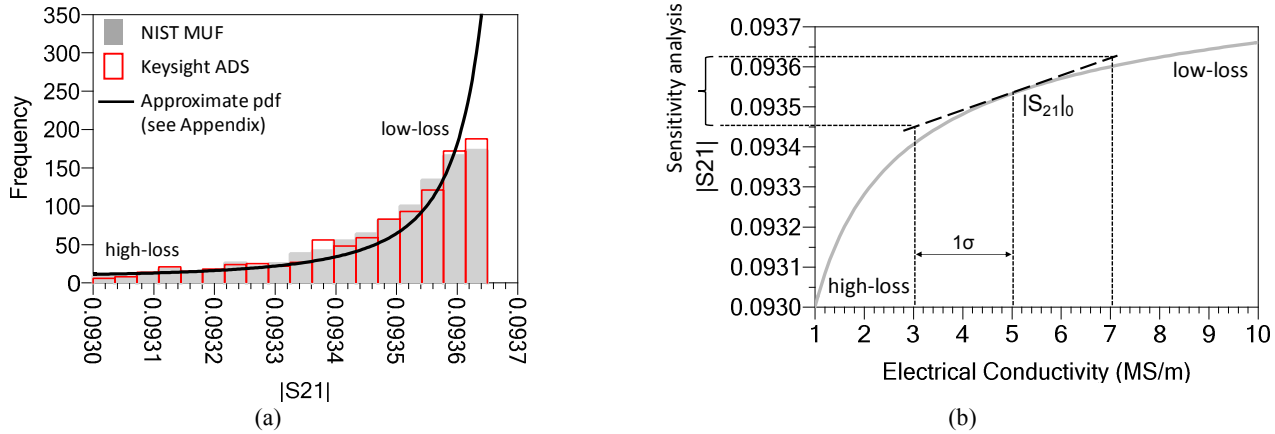

Fig. 7: Histogram of the magnitude of S_{21} at 44 GHz resulting from 1000 Monte-Carlo simulations (a). In the same plot, we show an approximate *pdf* (continuous line), derived analytically as explained in the Appendix. The area of the approximate *pdf* is normalized to the histogram area. In (b) we show the magnitude of calibrated S_{21} at 44 GHz, as a function of electrical conductivity of the coaxial line which models the open standard. The long-dashed line in (b) graphically indicates how the first-order approximation around the nominal value underlying the sensitivity analysis varies from the electrical conductivity beyond the region of the nominal value.

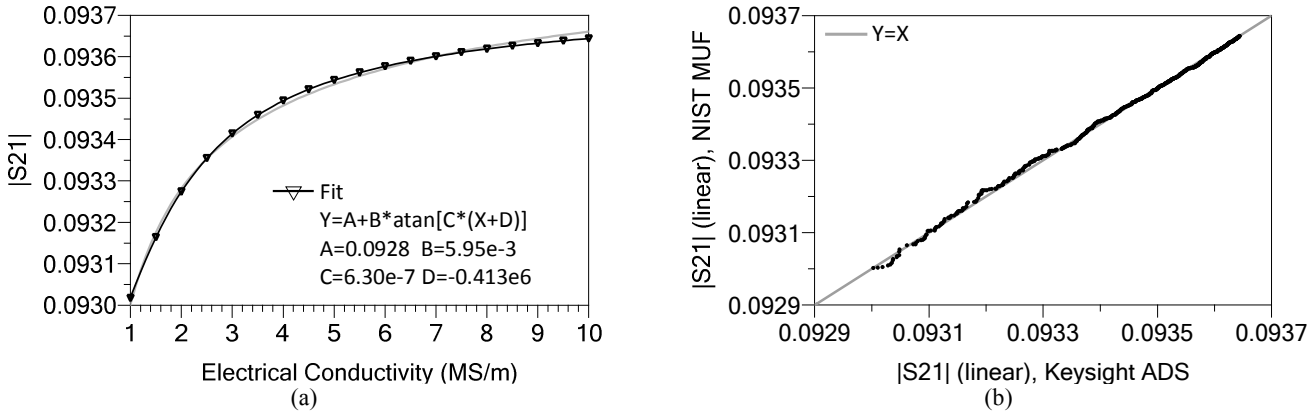

Fig. 8: Approximate fit (symbols) of the function in Fig. 7b (continuous grey line) (a) and q-q plot (dots) of the histograms of Fig. 7a (b). The grey continuous line in (b) depicts the line which the dots would lie on if the histograms in Fig. 7a were exactly the same.